Anomalous scaling of mortar fracture surfaces

Guillaume Mourot,[1,2] Stéphane Morel,[1,*] Elisabeth Bouchaud,[2] and Gérard Valentin[1]
[1]*LRBB, UMR 5103 (CNRS/INRA/Université Bordeaux 1), 69 route d'Arcachon, 33612 Cestas Cedex, France*
[2]*CEA-Saclay, DSM/DRECAM/SPCSI, 91130 Gif-Sur-Yvette Cedex, France*
(Received 26 August 2004; published 26 January 2005)

Scaling properties of mortar crack surfaces are studied from a mode I fracture test. Fracture surfaces initiated from a straight notch are shown to display an anomalous dynamic scaling of the crack roughness emphasizing the different crack developments between the directions parallel and perpendicular to the crack propagation direction. This anomalous roughening involves the existence of two different and independent roughness exponents. The first one, called the local roughness exponent ζ_{loc}, drives the self-affine scaling properties of the roughness perpendicular to crack propagation direction and can be considered as a universal roughness index $\zeta_{loc} \approx 0.8$. The second one, called the global roughness exponent, estimated to $\zeta \simeq 1.3$, is used to described the growth of the roughness at large length scales as a function of the distance to the initial notch and appears as a material-dependent parameter. We argue that the anomalous scaling of the roughness development could be an inheritance of the microcracked fracture process zone, quite large in quasibrittle materials. Finally, in the case of such an anomalous roughening, we argue that the fractal dimension appears insufficient to characterize the fracture surface morphology as a whole.

DOI: 10.1103/PhysRevE.71.016136 PACS number(s): 62.20.Mk

I. INTRODUCTION

The failure of quasibrittle materials such as mortars is characterized by the development of a microcracked fracture process zone ahead of the main crack. From a mechanical point of view, damage development in this fracture process zone leads to specific properties such as the resistance curve (*R*-curve) behavior and size effect. Concurrently, the elastic interactions which take place in the fracture process zone are known to have a strong influence on the local deviations of the main crack and, hence, on the resulting morphology of the fracture surfaces. Quantitative fractography appears in consequence to be a useful tool for the understanding of fracture mechanisms in quasibrittle materials.

Since the 1990s, many works have been dedicated to the statistical characterization of the morphology of fracture surfaces obtained for various loading conditions, and for materials as different as metallic alloys [1–4], ceramics [5,6], glass [7], rocks [8,9], sea ice [10], and wood [11–13]. They have shown that fracture surfaces exhibit self-affine scaling properties in a large range of length scales along the direction perpendicular to the direction of crack propagation (see Bouchaud [14,15] for reviews). In most cases, and in spite of huge differences in the fracture mechanisms, a roughness index $\zeta_{loc} \approx 0.8$, called the local roughness exponent, has been reported. It is now generally admitted that this local roughness exponent ζ_{loc} might have a universal value [1], i.e., independent of the fracture mode and of the material.

Moreover, several other recent studies that focused on the roughness development of fracture surfaces in quasibrittle materials [9,12,13] have shown that the roughness evolves as a function of the distance from the initial notch and must be described by an *anomalous* scaling law [16–18]. This law introduces two more exponents: the global roughness exponent ζ, which controls the roughness growth at large length scales, and the dynamical exponent z, which controls the increase of the self-affine correlation length as a function of the distance y to the initial notch. Anomalous scaling emphasizes especially the anisotropy of the crack developments in the directions parallel and perpendicular to the direction of crack propagation.

In this study, on the basis of the previous works of López and Schmittbuhl [9] and Morel *et al.* [12] on two quasibrittle materials (granite and wood, respectively), the morphology of fracture surfaces of a mortar was studied using quantitative fractography. We show that mortar fracture surfaces exhibit self-affine scaling properties, but also that the roughness of these surfaces is anisotropic and must be described on the basis of anomalous scaling. Finally, we argue that, in the case of anomalous roughening, the fractal dimension is insufficient to characterize completely the fracture surface; it only provides partial information, which does not allow us to account for the roughness development in the direction of crack propagation.

II. EXPERIMENT

The fracture surfaces are obtained from mortar notched beams subjected to four points bending (Fig. 1) leading to a mode I failure. The length of the beam is 1400 mm and its height and thickness are both equal to 140 mm. The initial notch is performed with a steel sheet (thickness 0.4 mm) pulled out when the mortar is 24 h old. The notch length is fixed to 70 mm, which corresponds to half the beam height. Note that the *R*-curve behavior of the mortar and the fact that the fracture tests were performed under displacement control lead to a mode I stable crack growth for the first 10–15 mm of the crack propagation. Hence, the crack velocity can be considered as approximately constant in this range. Such a

*Electronic address: morel@lrbb.u-bordeaux.fr

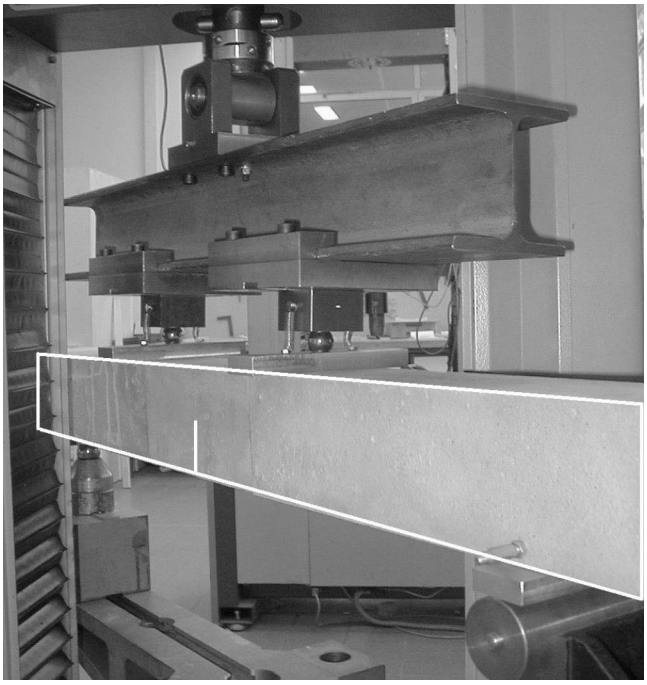

FIG. 1. Four points bending test of a mortar specimen. The sample edges and the initial notch have been outlined for clarity.

fracture test can be considered as quasistatic. On the other hand, the mortar is constituted by a sand for which the grain size ranges between 0.1 and 1.8 mm, and by high strength Portland cement.

The topography of the fracture surfaces has been recorded using an optical profilometer. The maps are built up with 500 profiles of 4096 points parallel to the initial notch (x direction, see Fig. 2). The sampling step along profiles (x direction) is 20 μm. The first profile, the roughness of which is approximately zero, lies close to the straight notch. Two successive profiles are separated by 50 μm along the direction of crack propagation (y direction). As the distance y to the initial notch increases, the magnitude of the roughness develops up to 7 mm. The lateral precision (along the x and y directions) is 2 μm, while the vertical accuracy, estimated from the height differences between two successive profiles along the same line, is approximately 5 μm.

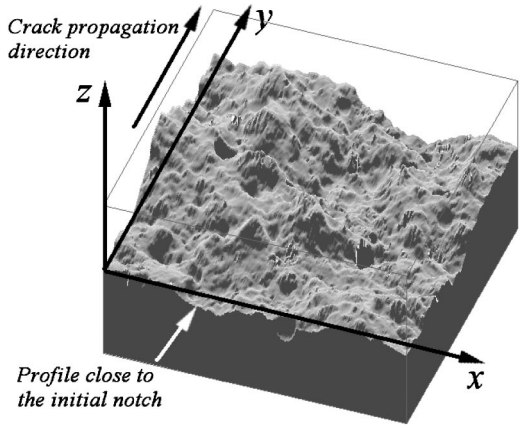

FIG. 2. Topography of a mortar fracture surface. The side length of this map is 130 mm.

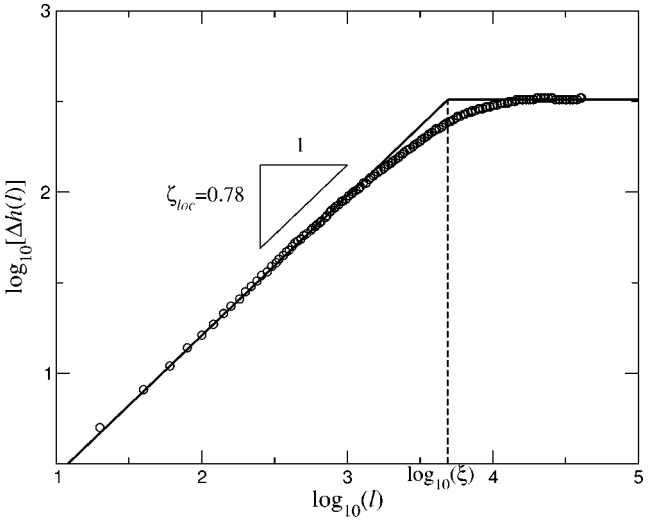

FIG. 3. Roughness Δh as a function of the length scale l for specimen m-03. The inclined straight line corresponds to the power law $\Delta h(l,y) \sim l^{\zeta_{loc}}$ and leads to the local roughness exponent $\zeta_{loc} = 0.78$. The horizontal straight line corresponds to the saturation of the roughness for length scales larger than the self-affine correlation length ξ.

III. SELF-AFFINE SCALING PROPERTIES: LOCAL ROUGHNESS EXPONENT

In order to determine the local roughness exponent ζ_{loc}, three independent methods have been used: the "variable bandwidth" method, the power spectrum, and the averaged wavelet coefficient method.

The "variable bandwidth" method consists in computing first the root mean square (RMS) $\Delta h(l)$ of the fluctuations of the height $z(x)$ over a window size l along the x axis. This quantity is then averaged over all possible origins j of the window along the profile [14,19],

$$\Delta h(l) = \left\langle \frac{1}{l}\sum_{i=1}^{l} z(x_i)^2 - \left(\frac{1}{l}\sum_{i=1}^{l} z(x_i) \right)^2 \right\rangle_j^{1/2}. \qquad (1)$$

As shown in Fig. 3, in the case of the specimen m-03 (Table I), the RMS roughness [Eq. (1)], estimated for a profile at a given position y from the initial notch, exhibits self-affine scaling properties

$$\Delta h(l, y = \text{const}) \sim \begin{cases} l^{\zeta_{loc}} & \text{if } l \ll \xi, \\ \text{const} & \text{if } l \gg \xi, \end{cases} \qquad (2)$$

where ξ is the self-affine correlation length along the x axis, below which the height fluctuations exhibit a power-law behavior characterized by the so-called local roughness exponent ζ_{loc}. According to Eq. (2) and as shown in Fig. 3, the magnitude of roughness saturates for length scales l larger than ξ.

The second method is the power spectrum (PSD), which is the squared amplitude of the autocorrelation function Fourier transform $\langle z(x+\Delta x)z(x)\rangle$. As shown in Fig. 4, for the same profile as the one used for the RMS roughness (specimen m-03), the power spectrum scales as

TABLE I. Values of the scaling exponents ζ_{loc}, ζ, and z. The local roughness exponent ζ_{loc} is estimated from the "variable bandwidth" method (RMS), the power spectrum (PSD), and the averaged wavelet coefficient (AWC) methods. The global roughness exponent ζ and dynamical exponent z are estimated from the scaling functions $g(u)$ [Eq. (7)] and $s(u)$ [Eq. (9)] related, respectively, to the scalings of the roughness RMS [Eq. (5)] and of the power spectrum PSD [Eq. (8)].

Specimen label	ζ_{loc}			$g(u)$ (RMS)		$s(u)$ (PSD)		ξ_{sat} (mm)
	RMS	PSD	AWC	ζ	z	ζ	z	
m-01	0.74	0.73	0.82	1.2	5.5	1.3	5.8	12.2
m-02	0.76	0.75	0.82	1.4	5.2	1.4	4.1	11.8
m-03	0.78	0.78	0.81	1.3	3.4	1.2	3.5	7.3
m-04	0.75	0.73	0.74	1.3	5.6	1.2	4.2	11.5
Average	0.76±0.04	0.75±0.05	0.80±0.05	1.3±0.1	4.9±0.20	1.3±0.10	4.4±0.20	10.7
	$\zeta_{loc}\simeq 0.77$		$\zeta\simeq 1.30$		$z\simeq 4.7$		$\xi_{sat}\simeq 10.7$mm	

$$S(k) \sim k^{-(2\zeta_{loc}+1)}, \tag{3}$$

where k is the wave vector [19].

The third independent method is the averaged wavelet coefficient method (AWC) [20]. This method consists of the average of the wavelet transform (*Daubechies* wavelet) of the data over the translation factor. In the case of a self-affine profile, the averaged wavelet coefficients $W[z](a)$, where a is the scale factor, are expected to scale as

$$W[z](a) \sim a^{1/2+\zeta_{\mathrm{loc}}}, \tag{4}$$

as shown in Fig. 5 in the case of the specimen *m*-03.

The estimates of the local roughness exponent values obtained with these three independent methods and for all tested specimens are given in Table I. Note that the local roughness exponent ζ_{loc} is determined on profiles located far from the initial notch, i.e., for large y values. The averages of the ζ_{loc} values obtained from all specimens lead to $\zeta_{loc}=0.76\pm0.04$ for the RMS method [Eq. (1)], 0.75 ± 0.05 for the power spectrum [Eq. (3)], and 0.80 ± 0.05 for the averaged wavelet coefficient method [Eq. (4)]. These values of ζ_{loc} are in agreement with the assumption of a universal value of this exponent, i.e., $\zeta_{loc}\approx 0.8$ for the three-dimensional fractures [1].

In the following, results on specimen *m*-03 are used as illustrations of the roughness development of mortar crack surfaces. Complete results for all specimens are provided in Table I.

IV. ROUGHNESS DEVELOPMENT: ANOMALOUS SCALING

If the roughness of the fracture profiles parallel to the x axis (see Fig. 2) can be described with a single roughness exponent (the universal local roughness exponent ζ_{loc}), it is not the case for profiles parallel to the direction of crack propagation. Indeed, as shown in Fig. 6 in the case of the specimen *m*-03, the RMS roughness grows as a function of the distance y to the initial notch from approximately zero

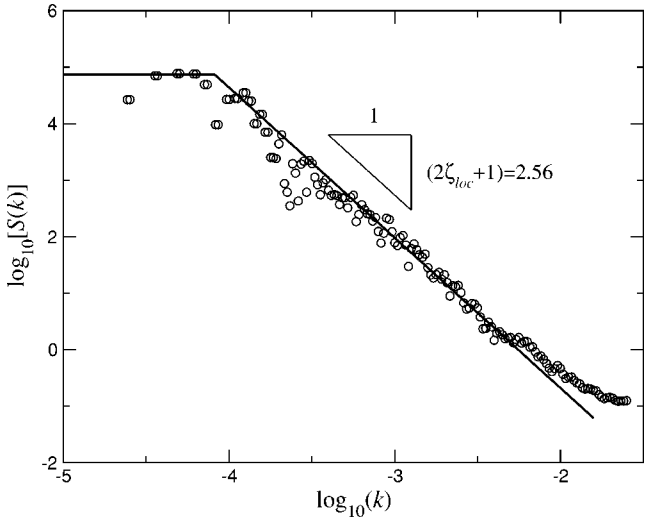

FIG. 4. Log-log plot of the power spectrum $S(k)$ in the case of specimen *m*-03. The straight line is relative to the power law $a^{(1/2+\zeta_{loc})}$ and leads to the local roughness exponent estimate $\zeta_{loc}=0.78$.

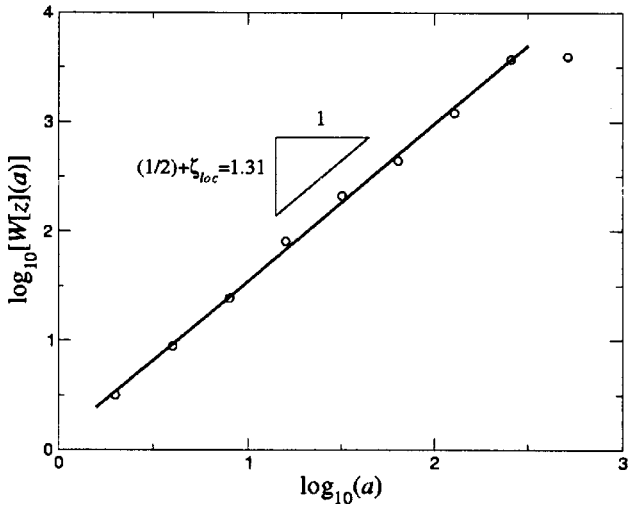

FIG. 5. Log-log plot of averaged wavelet coefficient $W[z](a)$ for specimen *m*-03. The slope of the straight line allows us to estimate the local roughness exponent $\zeta_{loc}=0.81$.

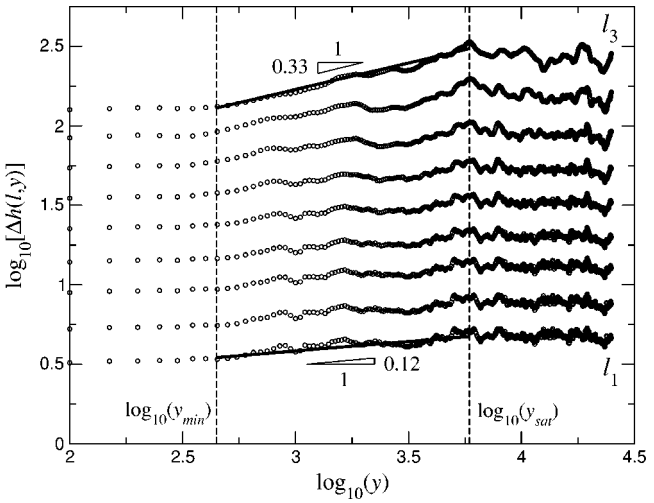

FIG. 6. Roughness RMS as a function of the distance y to the initial straight notch in the case of specimen m-03. The roughness growth domain is ranging between the positions y_{min} and y_{sat} (indicated by the dashed lines). The lower line corresponds to the fit of the roughness growth for a small length scale $[l_1 \ll \xi(y)]$ for all values of y. The nonzero slope is characteristic of the anomalous scaling.

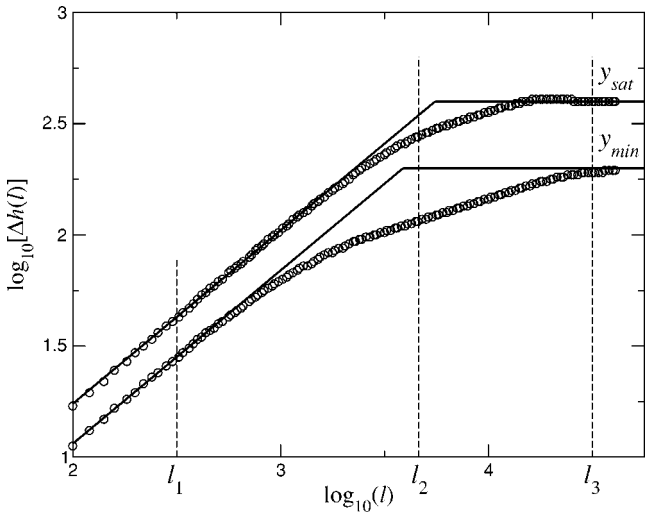

FIG. 7. RMS roughness as a function of length scale l for two profiles of specimen m-03 located (i) at the beginning of the domain of growing roughness, i.e., $y \approx y_{min}$, and (ii) when the global saturation of the roughness occurs, i.e., $y \approx y_{sat}$. $l_1 < \xi(y_{min}) < \xi(y_{sat})$, $\xi(y_{min}) < l_2 < \xi(y_{sat})$, and $\xi(y_{sat}) < l_3$.

for profiles close to the initial straight notch; profiles become rougher as the distance y increases. Note that in Fig. 6, the roughness growth is essentially observed for y values ranging between y_{min} and y_{sat}. For $y \ll y_{min} \simeq 0.5$ mm, the roughness magnitude is approximately constant because the nonzero thickness of the initial notch (0.4 mm) imposes a nonzero roughness at the onset of crack propagation. For $y \gg y_{sat} \simeq 5.8$ mm, the roughness magnitude saturates for all scales of observation. This will be discussed below. Moreover, it can be observed in Fig. 6 that the roughness increases differently at small (l_1) or at large length scales (l_3). In an equivalent way, such a phenomenon can be observed from Fig. 7, in which the RMS roughness obtained for two profiles corresponding approximately to positions y_{min} and y_{sat} is plotted. Note that the roughness of the profiles at y_{min} and y_{sat} is in agreement with Eq. (2). Figure 7 shows clearly that the roughness growth is linked to the increase of the self-affine correlation length ξ, which is larger for the profile at position y_{sat} than for the one at position y_{min}. This roughness growth appears also linked to a vertical shift of the curve corresponding to position y_{sat} with respect to the one at position y_{min}. Such a vertical shift can be obtained by increasing the prefactor in Eq. (2) as a function of the distance y to the initial notch. Hence, it appears clearly in Fig. 7 that the roughness estimated for a small length scale l_1 and for a larger one l_3 evolves differently with y. This reflects the difference in slopes observed in Fig. 6 for l_1 and l_3, as previously mentioned.

The scaling laws involved in the roughness development are similar to those observed in several models of nonequilibrium kinetic roughening [16,17,21–25]. In these examples, roughening does not follow the usual Family-Vicsek dynamic scaling law [26]. The difference in behavior of the small and large length scale height fluctuations have led to the introduction of a more general dynamic scaling hypothesis known as *anomalous* scaling [16–18]. In the case of the RMS roughness [Eq. (1)], the anomalous scaling can be described as follows:

$$\Delta h(l,y) \simeq A \begin{cases} l^{\zeta_{loc}} \xi(y)^{\zeta - \zeta_{loc}} & \text{if } l \ll \xi(y), \\ \xi(y)^{\zeta} & \text{if } l \gg \xi(y), \end{cases} \tag{5}$$

where the increase of the self-affine correlation length ξ as a function of the distance to the initial notch y follows a power law: $\xi(y) \sim y^{1/z}$, where z is called the dynamical exponent. Moreover, according to Eq. (5), there exist two regimes of roughness development along the y axis: for large length scales, i.e., $l \gg \xi(y)$, the roughness grows as $\Delta h(l,y) \sim y^{\zeta/z}$, where ζ is called the global roughness exponent while, for small length scales, i.e., $l \ll \xi(y)$, the roughness growth is characterized by the exponent $(\zeta - \zeta_{loc})/z$. Therefore, in the case of anomalous scaling, two more exponents ζ and z are needed to describe the surface. Note that the global roughness exponent ζ is different from and independent of the universal local one ζ_{loc}. It has been shown in previous experimental studies [9,12,13] that this exponent is a material-dependent parameter. On the other hand, when $\zeta = \zeta_{loc}$, small and large scales behave in the same way, and the scaling of the surface corresponds to the usual Family-Vicsek one [26],

$$\Delta h(l,y) \simeq A \begin{cases} l^{\zeta_{loc}} & \text{if } l \ll \xi(y), \\ \xi(y)^{\zeta_{loc}} & \text{if } l \gg \xi(y). \end{cases} \tag{6}$$

On the other hand, the anomalous scaling (or the Family-Vicsek one) is usually expressed as a function of time instead of position y. However, as previously mentioned, the crack velocity in our study can be considered as approximately constant and hence we assume a linear relationship between the position y of the profiles and time. Consistently, the topographic profiles can be considered as the successive positions of the advancing crack front.

According to the anomalous scaling law [Eq. (5)], the upper solid line in Fig. 6 corresponds to a fit of the roughness growth, between positions y_{min} and y_{sat}, for a large length scale, i.e., $l_3 \gg \xi(y)$ whatever the value of y. The slope of this line provides an estimate of the ratio $\zeta/z \simeq 0.33$. The lower line is a fit of the roughness observed for a small length scale, i.e., $l_1 \ll \xi(y)$ for all values of y, and, according to Eq. (5), it provides an estimate of the exponent $(\zeta-\zeta_{loc})/z \simeq 0.12$ which is significantly larger than zero. This dependence of the roughness at the smallest length scales as a function of the crack advance y is characteristic of the anomalous scaling behavior. It differs from the Family-Vicsek one for which, according to Eq. (6) for $l \ll \xi(y)$, the roughness is expected to be independent of y for small length scales. Moreover, for an intermediate length scale l_2, i.e., ranged between l_1 and l_3 as shown in Fig. 7, both roughness growth regimes should be observed as a function of the distance y in Fig. 6. Indeed, from a theoretical point of view, according to Eq. (5) and as shown from the asymptotes plotted in Fig. 7, for position y just above y_{min}, the self-affine correlation length being smaller than l_2, the roughness growth regime should be characterized by the exponent ζ/z. In the same way, for positions y close to y_{sat}, the self-affine correlation length ξ becoming larger than l_2, the roughness growth regime should be driven by the exponent $(\zeta-\zeta_{loc})/z$. However, in Fig. 6, both theoretical regimes cannot be clearly observed for any intermediate length scale l_2 because of the existence of a crossover regime between the self-affine and the saturation regimes (as shown, for instance, in Fig. 7). As a consequence, in Fig. 6, only a progressive increase of the slope, from $(\zeta-\zeta_{loc})/z$ to ζ/z, can be observed as a function of the length scales ranging between l_1 and l_3.

On the other hand, as shown in Fig. 6, for positions $y \geqslant y_{sat}$, the roughness saturates at all length scales. This is linked to the fact that the self-affine correlation length has reached its maximum value, i.e., $\xi(y \geqslant y_{sat}) = \xi_{sat}$, and hence according to Eq. (5), the magnitude of the roughness is expected to stay constant for all values of l and $y \geqslant y_{sat}$. Note that the maximum self-affine correlation length has been estimated to be about 8% of the beam width, i.e., $\xi_{sat} \simeq 10.7$ mm, which exceeds the maximum grain size (Table I).

Thus, as the local roughness exponent value is estimated to be $\zeta_{loc}=0.78$ in the case of specimen m-03, the slopes corresponding to the upper and the lower lines in Fig. 6, respectively, $\zeta/z = \simeq 0.33$ and $(\zeta-\zeta_{loc})/z \simeq 0.12$, lead to a first estimate of the global roughness exponent and the dynamical exponent values $\zeta \simeq 1.20$ and $z \simeq 3.7$.

On the other hand, in order to confirm the values of the global roughness exponent ζ and of the dynamical exponent z, it is useful to define a scaling function for the behavior of the RMS roughness $\Delta h(l,y)$, defining $g(u)$ as $g(l/y^{1/z}) = \Delta h(l,y)/l^{\zeta}$ [18]. From Eq. (5), $g(u)$ is expected to scale as

$$g(u) \sim \begin{cases} u^{-(\zeta-\zeta_{loc})} & \text{if } u \ll 1, \\ u^{-\zeta} & \text{if } u \gg 1. \end{cases} \tag{7}$$

For all profiles ranging between positions y_{min} and y_{sat}, the experimental values of $g(u)$ (where $u=l/y^{1/z}$) have been computed for various values of the scaling exponents ζ and z. As shown in Fig. 8 for the specimen m-03, the best data collapse is obtained for the scaling exponents, $\zeta = 1.30 \pm 0.10$ and $z = 3.4 \pm 0.2$ (Table I), which are in good agreement with the first estimates of these values previously obtained from the roughness growth regimes at small and large length scales in Fig. 6.

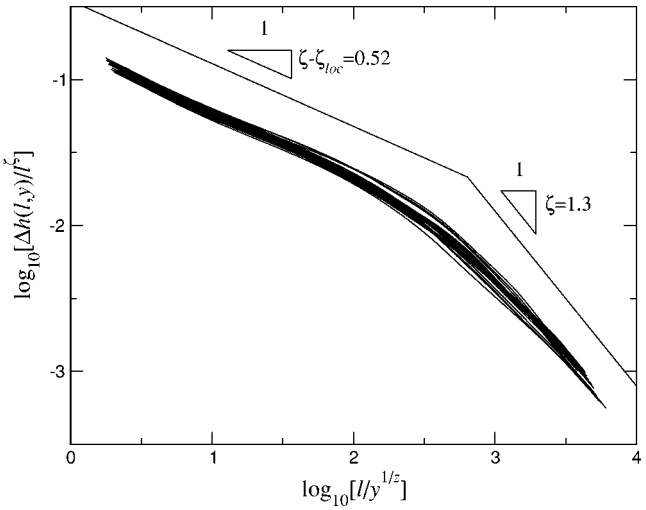

FIG. 8. Roughness RMS data collapse of the profiles ranging between y_{min} and y_{sat} obtained for the scaling exponents $\zeta=1.3$ and $z=3.4$ (specimen m-03). Scaling is in good agreement with Eq. (7).

The scaling exponents ζ and z can also be estimated independently using the power spectrum data defined in Eq. (3). Indeed, in the case of the anomalous scaling, the power spectrum is known to scale as [9,18,23–25]

$$S(k,y) \sim k^{-(2\zeta+1)} s(ky^{1/z}), \tag{8}$$

where s is the scaling function

$$s(u) \sim \begin{cases} u^{2\zeta+1} & \text{if } u \ll 1, \\ u^{2(\zeta-\zeta_{loc})} & \text{if } u \gg 1. \end{cases} \tag{9}$$

As for the RMS roughness, the experimental values of $s(u)$ (where $u=ky^{1/z}$) have been computed for different values of the scaling exponents ζ and z in the case of specimen m-03 for profiles located between y_{min} and y_{sat}. For the power spectrum, the best data collapse is obtained for the values $\zeta = 1.20 \pm 0.1$ and $z = 3.5 \pm 0.2$ (Fig. 9), which are in very good agreement with those obtained from the RMS roughness (Table I).

Similar results have been obtained for all the tested specimens as shown in Table I. Note that the values of the global roughness exponent ζ and of the dynamical exponent z obtained from the scaling of the RMS roughness are consistent with those obtained from the scaling of the power spectrum. Nevertheless, if the value of the global roughness exponent appears to be quite robust, the average of the values obtained from the RMS and PSD scalings leading to $\zeta \simeq 1.3 \pm 0.10$, the dynamical exponent values are more scattered, with an estimated average $z \approx 4.7$.

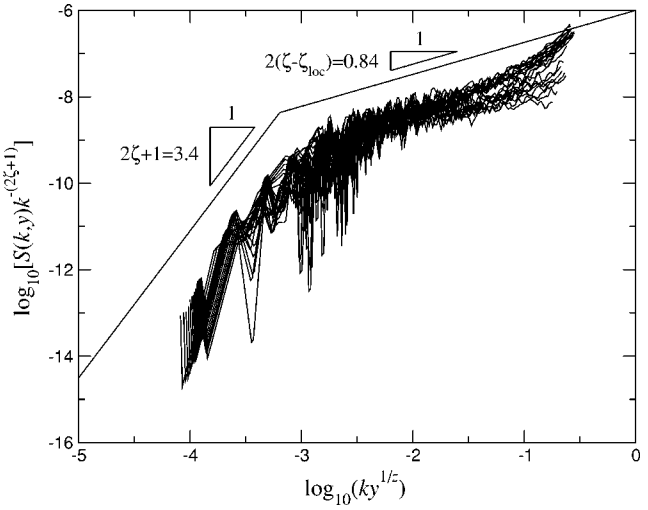

FIG. 9. Power spectrum data collapse of the profiles ranging between y_{min} and y_{sat} in the case of specimen *m*-03. The best collapse is obtained for $\zeta=1.20$ and $z=3.5$. Scaling is consistent with Eq. (9).

Thus, as expected from the results obtained for two other quasibrittle materials (granite [9] and wood [12]), a mortar fracture surface also exhibits anomalous roughening. Table II summarizes the values of ζ and z found for granite [9] and several wood species [12]. The anomalous scaling could be an inheritance of the diffuse damage (fracture process zone) which progressively develops ahead of the crack front in quasibrittle material (and whose *R*-curve behavior is the mechanical consequence). Indeed, as previously mentioned in the Introduction, the more or less long-range elastic interactions which take place in the fracture process zone and, especially, the fact that the intensity of these interactions evolves as a function of the crack advance, must have a strong influence on the local deviations of the main crack, and so they could explain the roughness growth at small length scales (characteristic of the anomalous scaling). On the contrary, the crack surfaces, arising from a more localized fracture process, could exhibit a roughness development closer to a Family-Vicsek one (or in other terms *weakly* anomalous). However, such hypotheses should be confirmed from roughness development analysis in materials such as glass, for instance, whose fracture process is well known to be very localized.

TABLE II. Global roughness exponent ζ and dynamical exponent z values obtained from different quasibrittle materials

	Maritime pine [12]	Norway spruce [12]	Granite [9]	Mortar
Global roughness exponent ζ	1.35	1.60	1.20	1.30
Dynamical exponent z	2.3	3.0	1.2	4.7

V. CONCLUSION

Along the direction parallel to the initial notch, the roughness of mortar fracture surfaces exhibits a self-affine scaling behavior characterized by the local roughness exponent $\zeta_{loc} \approx 0.8$ which is consistent with the assumption of universality [1]. The results reported here on mortar confirm that the roughness development of fracture surfaces of quasibrittle materials is anisotropic and follows an anomalous scaling law. The anomalous scaling requires the introduction of two more exponents: the global roughness exponent ζ, which controls the growth of the roughness at large length scales as a function of the distance to the initial notch, and the dynamical exponent z, which describes the growth of the correlation length.

A comparison of our results with previous experimental results obtained on other quasibrittle materials (granite [9] and wood [12]) suggests that the anomalous scaling could be a consequence of the development of the fracture process zone characteristic of these quasibrittle materials. Finally, the fractal dimension defined as $d_F=d_T+1-\zeta_{loc}$, where d_T is the topological dimension and which is frequently used to describe the morphology of fracture surfaces, appears insufficient to characterize completely the crack surface morphology in the case of anomalous roughening.

ACKNOWLEDGMENT

This work has received financial support from the Région Aquitaine.

[1] E. Bouchaud, G. Lapasset, and J. Planés, Europhys. Lett. **13**, 73 (1990).
[2] R. H. Dauskardt, F. Haubensk, and R. O. Ritchie, Acta Metall. Mater. **38**, 143 (1990).
[3] A. Imre, T. Pajkossy, and L. Nyikos, Acta Metall. Mater. **40**, 1819 (1992).
[4] S. Morel, T. Lubet, J.-L. Pouchou, and J.-M. Olive, Phys. Rev. Lett. **93**, 065504 (2004).
[5] J. J. Mecholsky, D. E. Passoja, and K. S. Feinberg-Ringel, J. Am. Ceram. Soc. **72**, 60 (1989).
[6] K. J. Måløy, A. Hansen, E. L. Hinrichsen, and S. Roux, Phys. Rev. Lett. **68**, 213 (1992).
[7] P. Daguier, B. Nghiem, E. Bouchaud, and F. Creuzet, Phys. Rev. Lett. **78**, 1062 (1997).
[8] J. Schmittbuhl, F. Schmitt, and C. Scholz, J. Geophys. Res. **100**, 5953 (1995b).
[9] J. M. López and J. Schmittbuhl, Phys. Rev. E **57**, 6405 (1998).
[10] J. Weiss, Eng. Fract. Mech. **68**, 1975 (2001).
[11] T. Engøy, K. J. Måløy, A. Hansen, and S. Roux, Phys. Rev. Lett. **73**, 834 (1994).
[12] S. Morel, J. Schmittbuhl, J. M. López, and G. Valentin, Phys. Rev. E **58**, 6999 (1998).

[13] S. Morel, G. Mourot, and J. Schmittbuhl, Int. J. Fract. **121**, 23 (2003).
[14] E. Bouchaud, J. Phys.: Condens. Matter **9**, 4319 (1997).
[15] E. Bouchaud, Surf. Rev. Lett. **10**, 73 (2003).
[16] J. M. López and M. A. Rodríguez, Phys. Rev. E **54**, R2189 (1996).
[17] J. M. López, M. A. Rodríguez, and R. Cuerno, Phys. Rev. E **56**, 3993 (1997a).
[18] J. M. López, M. A. Rodríguez, and R. Cuerno, Physica A **246**, 329 (1997b).
[19] J. Schmittbuhl, J.-P. Vilotte, and S. Roux, Phys. Rev. E **51**, 131 (1995a).
[20] I. Simonsen, A. Hansen, and O. M. Nes, Phys. Rev. E **58**, 2779 (1998).
[21] M. Schroeder, M. Siegert, D. E. Wolf, J. D. Shore, and M. Plischke, Europhys. Lett. **24**, 563 (1993).
[22] S. Das Sarma, S. V. Ghaisas, and J. M. Kim, Phys. Rev. E **49**, 122 (1994).
[23] J. Soriano, J. Ortín, and A. Hernández-Machado, Phys. Rev. E **67**, 056308 (2003).
[24] J. Soriano, J. J. Ramasco, M. A. Rodríguez, A. Hernández-Machado, and J. Ortín, Phys. Rev. Lett. **89**, 026102 (2002).
[25] J. J. Ramasco, J. M. López, and M. A. Rodríguez, Phys. Rev. Lett. **84**, 2199 (2000).
[26] F. Family and T. Vicsek, *Dynamics of Fractal Surfaces* (World Scientific, Singapore, 1991).